PCCP

PAPER

View Article Online
View Journal | View Issue

Density functional theory studies of methyl dissociation on a Ni(111) surface in the presence of an external electric field

Cite this: *Phys. Chem. Chem. Phys.*, 2014, **16**, 2399

Fanglin Che,[a] Renqin Zhang,[a] Alyssa J. Hensley,[a] Su Ha[a] and Jean-Sabin McEwen*[ab]

Received 1st October 2013,
Accepted 28th November 2013

DOI: 10.1039/c3cp54135e

www.rsc.org/pccp

To provide a basis for understanding the reactive processes on nickel surfaces at fuel cell anodes, we investigate the influence of an external electric field on the dehydrogenation of methyl species on a Ni(111) surface using density functional theory calculations. The structures, adsorption energies and reaction barriers for all methyl species dissociation on the Ni(111) surface are identified. Our results show that the presence of an external electric field does not affect the structures and favorable adsorption sites of the adsorbed species, but causes the adsorption energies of the CH_x species at the stable site to fluctuate around 0.2 eV. Calculations give an energy barrier of 0.692 eV for $CH_3^* \rightarrow CH_2^* + H^*$, 0.323 eV for $CH_2^* \rightarrow CH^* + H^*$ and 1.373 eV for $CH^* \rightarrow C^* + H^*$. Finally, we conclude that the presence of a large positive electric field significantly increases the energy barrier of the $CH^* \rightarrow C^* + H^*$ reaction more than the other two reactions, suggesting that the presence of pure C atoms on Ni(111) are impeded in the presence of an external positive electric field.

1. Introduction

Solid oxide fuel cells (SOFC) constitute an attractive power-generation technology that converts the chemical energy of various logistic fuels directly into electricity, while maintaining a high electrical efficiency and causing little pollution through electrochemical processes.[1,2] The SOFC system is a widely studied system that uses methane as its fuel, mainly because it is abundantly available in natural gas and is a simple compound to model.[3] Recently, shale gas has received a tremendous amount of interest as a new future energy source.[4] In the future, this shale gas can be directly fed into the SOFC system and it can be more efficiently converted into electrical energy than the conventional gas turbine rote.[5,6] Such a technology can contribute to the additional energy required for our future society with a "more electrical" platform. There are two main reactions that take place in a SOFC system, as shown below:[7,8]

$$CH_4 + H_2O \leftrightarrow CO + 3H_2 \quad (1)$$

$$CO + 3H_2 + 4O^{2-} \rightarrow CO_2 + H_2O + 8e^- \quad (2)$$

At the anode, the steam can be either co-fed with the fuel to impede the carbon deposition rate or produced as the byproduct from the electrochemical oxidation reaction. Under the presence of this steam, the steam-reforming reaction takes place to produce syngas. The syngas is then electrochemically oxidized by reacting with the lattice oxygen from the cathode, producing CO_2, H_2O, and electrons as products. These electrons flow through the external circuit to produce the net electrical power, and combine with gas phase oxygen at the cathode to produce the lattice oxygen and complete the electrical circuit. The rate-limiting step for this reforming reaction over the anode surface is the dissociative chemisorption of methane.[9]

Nickel (Ni) is the most commonly used catalyst in industrial steam reforming processes today, due to its economic advantage.[10] Currently, many researchers are investigating the sequential dehydrogenation of methane (CH_4) on a Ni catalyst at a molecular level in order to have a better understanding of the overall reaction mechanism. However, the main disadvantage of using Ni as a catalyst for this reaction is that the carbon–carbon bonds are easily formed even under the presence of steam on the Ni active surface and decreases the activity of the catalyst over the long operation time.[11]

In order to control the ongoing reactions in the SOFC, one can modify the selectivity of the Ni catalyst. Since CH_4 physisorbs on Ni,[12,13] various theoretical methods have focused more on the dissociative chemisorption of methyl species, providing important data concerning the thermodynamics of CH_x interconversion. Early studies show that the Ni(111) surface is the least reactive of the low index surfaces;[14] however, as the most

[a] *The Gene and Linda Voiland School of Chemical Engineering and Bioengineering, Washington State University, WA, 99164, USA. E-mail: js.mcewen@wsu.edu*
[b] *Department of Physics and Astronomy, Washington State University, WA, 99164, USA*

stable surface, most subsequent investigations were done for this surface. Mueller *et al.*[15] reported quantum mechanistic calculations of the equilibrium structures, C–H binding energies, and reaction barriers for methyl species on the Ni(111) surface. In this work, it was found that all methyl species prefer binding to the hollow sites and CH was the most stable form of CH_x on Ni(111) based on the results of the energy barriers. Nave *et al.*[16] investigated the effect of lattice motion and relaxation on the dissociative adsorption of methane on Ni(111) by carrying out highly dimensional fully quantum scattering calculations. From the results, it was found that a significant amount of lattice puckering occurs. This lattice puckering of about 0.2 Å lowers the reaction barriers for methane dissociation by 0.2 eV. Kratzer *et al.*[17] presented the first step of methane adsorption on the Ni(111) surface, the dissociation of CH_4 to adsorbed CH_3 and H over the pure Ni(111) and gold-alloyed Ni(111) surfaces. The results showed that alloying the surface with gold would increase reaction barriers by 0.166 and 0.394 eV for a Ni atom with one or two gold neighbors, respectively. Bengaard *et al.*[18] presented a detailed and comprehensive mechanistic picture of the steam reforming process and the nucleation of graphite on both the Ni(111) and Ni(211) surfaces. They found that certain step sites are considerably more reactive than close-packed facets for both reactions. They had also shown that the known promoters for this system, potassium, sulfur, and gold, preferentially bind to the step edges of Ni and suggested that this is the main reason for the suppression of graphite formation observed for these systems. Watwe *et al.*[19] performed periodic, infinite plane wave slab calculations to study the adsorption of CH_x species on a Ni(111) surface and also presented a potential energy diagram for the overall reaction of surface carbon with dihydrogen to methane, or equivalently the conversion of methane to surface carbon, including all adsorbed intermediates and transition states. Yang *et al.*[20] provided a detailed analysis of the vibrational spectra of CH_3, CH_2D, and CD_3 adsorbed on Ni(111) and the products of their reactions. Overall, the researchers have investigated the different factors that influence the decomposition of methane on the Ni(111) surface, including lattice motion, relaxation, adding gold, sulfur or potassium to the Ni surface, and altering the H to D of methane.

In the SOFC system, the presence of a large electric field, on the order of 1 V $Å^{-1}$, occurs near the electrode/electrolyte interface and is generated from the large electric potential drop, which results from the combined effects of electronic structure of the electrode, the adsorption species at the interface and the effective potential in the bulk solution.[21–23] As a result, the field applied in a SOFC is strong enough to induce rearrangements of electronic orbitals of atoms and molecules, leading to new phenomena that can be described as field-induced chemisorption. The presence of this large electric field is in fact another variable of state that influences the catalytic processes occurring at the electrode–electrolyte interface.[21,23] Therefore, in order to get a better understanding of the environmental and operating factors that impact a SOFCs system, it is crucial that we investigate to what extent an electric field alters the underlying reaction pathways and energy barriers.[24] Furthermore, this finding would benefit the design of future catalytic reactors, where the applied external electric field can significantly alter the reaction activity and selectivity.

In this paper, we will examine the reaction barriers involved in the dehydrogenation of methyl species on a Ni(111) surface using *ab initio* quantum chemistry methods. This study is aimed to provide: (1) a theoretical investigation based on density functional theory (DFT) from first principles on the stability and reactivity of CH_x species on the Ni(111) surface, (2) the reaction energy towards the dehydrogenation of methyl groups, and (3) the reaction barriers and reaction pathways for the decomposition of CH_x in the presence and the absence of large electric fields. For this work we used the reaction elementary steps as shown by eqn (3)–(5) to calculate the adsorption energies of the reactants and the products.

$$CH_3^* \rightarrow CH_2^* + H^* \quad (3)$$

$$CH_2^* \rightarrow CH^* + H^* \quad (4)$$

$$CH^* \rightarrow C^* + H^* \quad (5)$$

We will show the results of binding energies and the underlying adsorption configurations for CH_x species and H on the Ni(111) surface as obtained from DFT calculations on periodically infinite slabs with and without electric fields. We also report the pathways and energy barriers for the decomposition of CH_x to form CH_{x-1} and H on a Ni(111) surface. The computational methods and models used to evaluate this system are presented in Section 2. Section 3 gives the details of our computational results for the CH_x species adsorbed on the Ni(111) surface in the presence and the absence of external electric fields. It also covers the results regarding the external electric field effect on the energy barriers, transition state configurations, and reaction pathways for the dehydrogenation of CH_x. Additionally, we present a comprehensive mechanistic picture of methyl species dissociation on the Ni(111) surface with and without electric fields. Finally, Section 4 summarizes our findings and presents some conclusions.

2. Computational methods

The Vienna Ab initio Simulation package (VASP) was used to perform the DFT calculations with the generalized gradient approximation (GGA)[25,26] as parameterized by the Perdew–Wang 91 (PW91)[27] functional combined with the projector-augmented wave method for solving the Kohn–Sham equations.[28] The conjugate-gradient algorithm[29] was adopted to relax the ions into their ground state with the length of the trial step controlled by a force scaling constant of 0.1.

A four-layer metal slab was modeled using a $p(3 \times 3)$ supercell[30–32] (corresponding to a coverage of 1/9 ML) with the two bottom layers fixed at their equilibrium (*i.e.*, bulk phase positions), while the upper layers were allowed to relax. The Ni lattice constant was theoretically calculated and was found to be 3.521 Å, which is very close to the other theoretical calculation (3.522 Å[33]), and is within 0.08% of the experimental value of 3.524 Å.[34]

The periodically repeating unit cells were separated by 11 Å of vacuum. This is comparable to the values used in the literature, which range from 10 Å[35] to 12 Å[36] to ensure that adsorbates and the subsequent slab would have minimal interactions. A plane-wave basis set was expanded to a kinetic energy maximum of 400 eV for the Kohn–Sham orbitals. A first-order Methfessel–Paxton smearing method with width of 0.1 eV was used to account for partial occupancies around the Fermi level and to speed up the convergence.[37] The Brillouin zone integration was approximated by a sum over *k*-points chosen using a Monkhorst–Pack mesh[37] with a grid of (4 × 4 × 1) *k*-points. Geometries were considered optimized when the energy had converged to 10^{-4} eV and the forces were smaller than 0.03 eV $Å^{-1}$. In addition, all the calculations included spin-polarization effects due to the ferromagnetic nature of the Ni surface.[38]

To estimate the error based on *k*-point sampling, we calculated the adsorption energies for several (identical) structures using a (6 × 6 × 1) *k*-point sampling and compared to our *k*-point grid of (4 × 4 × 1). We found that the adsorption energies differed for H, CH, CH_2 and CH_3 changed by at most 0.010 eV. We also found that by increasing the cutoff energy from 400 eV to 450 eV for hydrogen and the hydrocarbons changed the adsorption energies by at most 0.016 eV.

The minimum energy pathways (MEP) between two specified configurations at their energy minima for the reaction studied here were calculated using the nudged elastic band (NEB) method.[39,40] This was done by introducing a number of "images", or adsorption configurations along the reaction pathway. When the reaction pathway had an energy minimum between the chosen initial and final steps, the configuration nearest the intermediate minimum point was relaxed to that minimum. This was done in order to verify that the local minimum was indeed present and to fully evaluate the reaction pathway. The original pathway was then separated into two segments based on the intermediated minimum and the reaction pathway was calculated for each segment. The MEPs were then refined using the climbing image nudged elastic band (CINEB) method.[41] The transition states (TS)[42] were further verified by calculating their vibrational frequencies confirming that a single unique normal mode eigenvector was obtained which corresponds to the negative curvature at the saddle point. Also, the dimer method was applied in searching the saddle point combined when the CINEB converged to a second order saddle point.[43]

The strength of each adsorption site was measured using the adsorption energy as defined:

$$E_{ads} = E_{(M/slab)} - E_{(M)} - E_{(slab)} \quad (6)$$

where $E_{(M/slab)}$ is the total energy of the slab with the chemisorbed atom on the surface, $E_{(M)}$ is the energy of the free molecule, and $E_{(slab)}$ is the energy of the bare slab of the surface. The reaction energy associated with the dissociative reaction of AB* → A* + B* was calculated based on two different definitions, including the separate reaction energy E_s, and co-adsorption reaction energy E_c given as follows:

$$E_s = (E_{(A/slab)} + E_{(B/slab)}) - (E_{(AB/slab)} + E_{(slab)}) \quad (7)$$

$$E_c = E_{((A+B)/slab)} - E_{(AB/slab)} \quad (8)$$

where $E_{(A/slab)}$, $E_{(B/slab)}$ and $E_{(AB/slab)}$ are the total energies for the adsorption of A, B and AB species, respectively. $E_{((A+B)/slab)}$ is total energy of co-adsorbed A and B on a Ni(111) surface. Here we use the convention that an exothermic reaction occurs for negative values of E_s while an endothermic reaction occurs for a positive value of E_s. Moreover, E_c will be used when calculating the overall minimum energy pathways.

3. Results and discussion

In this section, we report the results of the methyl species absorbed on the Ni(111) surface in the presence and absence of external electric fields, including the adsorption energies, site preferences, adsorption geometries, the effect of electric fields, and a comparison of our results with related papers and experiments. After reporting the isolated adsorption of methyl species on the Ni(111) surface, a thorough investigation on the three-stepped dissociative reaction of methyl will be presented. This will include the co-adsorption reaction energy of hydrocarbon species, reaction pathways and energy barriers both with and without external electric fields.

3.1 Adsorption of hydrogen on Ni(111)

For a single H atom, four adsorbed sites were considered, the top, bridge, fcc and hcp sites (initial configurations shown in Fig. 1). Our calculations show that the top, fcc, and hcp sites were stable geometries for the H atom with the adsorption energies given in Table 1. However, the initial bridge site was found to be unstable and the adsorbed atom shifted to the adjacent fcc site. We remark that the adsorption energy of an H atom at the hcp site is only 0.018 eV weaker than the most favorable fcc site. Despite these small differences, the designation of the most favorable site is in agreement with the results of Wang *et al.*[44] (see Table 1) where the GGA of Purdue, Burke and Ernzerhof (PBE) was used.[26] On the other hand, the differences in the absolute adsorption energy values can be attributed to the smaller $p(2 \times 2)$ unit cell that was used, which is smaller than what we used in our model. The increased size of our supercell

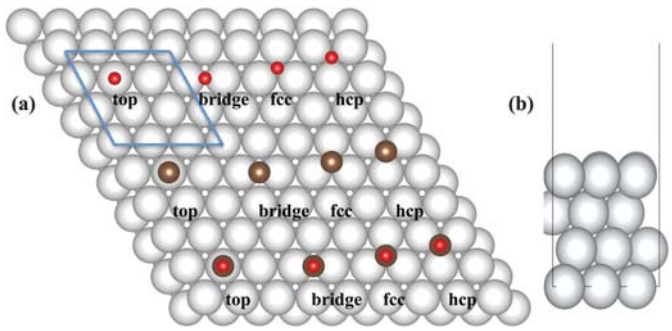

Fig. 1 Configurations considered for the adsorption of H, C, and CH species on the Ni(111) surface (from top to bottom): (a) shows the top view of the four layer Ni(111) surface with the high-symmetry binding sites identified along with the p(3 × 3) supercell and (b) shows the side views of the single unit cell. The light grey spheres (large) are Ni atoms, and brown spheres (medium) are C atoms, and the red spheres (small) are H atoms.

Table 1 Summary of methyl species adsorption energy data on the Ni(111) surface

Species	E_{ads} (eV)	Species	E_{ads} (eV)
H (top)	−2.247, −2.22[a], −2.29[e]	CH_2 (bridge1)	−3.968
H (bridge)	Unstable, −2.72[e]	CH_2 (bridge2)	−3.711, −3.64[e]
H (fcc)	−2.842, −2.77[a], −2.85[e]	CH_2 (fcc)	−4.227, −3.85[a], −4.18[b], −3.87[e]
H (hcp)	−2.824, −2.76[a], −2.86[b], −2.84[e]	CH_2 (hcp)	−4.178, −3.83[a], −3.84[e]
C (top)	−4.526, −4.49[e]	CH_3 (top1)	−1.736, −1.55[a], −1.491[d]
C (bridge)	Unstable, −6.21[e]	CH_3 (top2)	−1.737, −1.55[a], −1.491[d]
C (fcc)	−6.883, −6.52[a], −6.94[b], −6.353[c], −6.64[e]	CH_3 (top3)	−1.737, −1.489[d], −1.61[e]
C (hcp)	−6.939, −6.61[a], −7.02[b], −6.71[e]	CH_3 (bridge1)	−1.852, −1.609[d], −1.70[e]
CH (top)	Unstable, −4.32[e]	CH_3 (bridge2)	Unstable, −1.583[d]
CH (bridge)	Unstable, −6.05[e]	CH_3 (bridge3)	Unstable, −1.581[d]
CH (fcc)	−6.548, −6.27[a], −6.38[b], −6.42[e]	CH_3 (fcc1)	−2.055, −1.81[a], −1.97[b], −1.820[d], −1.85[e]
CH (hcp)	−6.534, −6.35[a], −6.46[e]	CH_3 (fcc2)	Unstable, −1.462[d]
CH_2 (top1)	Unstable	CH_3 (hcp1)	−2.016, −1.78[a], −1.788[d], −1.83[e]
CH_2 (top2)	−2.203, −2.78[a], −2.86[e]	CH_3 (hcp2)	Unstable, −1.438[d]

[a] From ref. 44. [b] From ref. 12. [c] From ref. 19. [d] From ref. 47. [e] From ref. 15.

model means that our binding energies should be slightly stronger as compared to their results if the lateral interactions are repulsive.

In addition to the above work, a study on the effect of an external electric field on the adsorption of a single H atom at the stable sites on a Ni(111) surface was conducted. Fig. 2 shows the electric field effect on the isolated H atom on the Ni(111) surface. From Fig. 2, it is clear that the electric field does not change the binding site preferences of an H atom. Since the fcc site was still the most stable adsorption site for an H atom, the effects of the external electric field for this site was further examined. In the absence of an electric field, the vertical distance between the surface and the adsorbed H atom at the fcc site is 0.902 Å above the Ni surface, which is shorter than that seen experimentally (1.15 ± 0.05 Å).[45] The Ni–H bond length was found to be 1.709 Å, which is in excellent agreement with Watwe's results[19] of 1.70 Å. After applying the large external electric field, the vertical distance and Ni–H bond length changed slightly by about 0.01 Å. It was also found that both the positive and negative electric fields decreased the adsorption energy of an H atom. When the external electric field was equal to 1.0 V Å^{-1}, the adsorption energy was −2.800 eV, which is 0.042 eV smaller than the adsorption energy of an H atom on the Ni(111) surface with no electric field present. We notice that the different adsorption energies depend on the magnitude of the local electric field. This dependence can be expanded in powers of the electric field as

$$E = E_0 + \vec{d}\cdot\vec{F} + \frac{\alpha}{2}F^2 \quad (9)$$

where $|\vec{d}|$ can be regarded as an effective dipole moment and α as effective polarizability.[46] The values of $|\vec{d}|$ and α are presented in Table 2. We remark that $|\vec{d}|$ is smaller than the estimated value of 0.040 eV Å V^{-1} for an H atom at the Rh catalyst. However, these two effective dipole moments are both positive, so that an applied positive external electric field weakens hydrogen's adsorption energies.

Table 2 Summary of the dipole moments ($\vec{d}$ in units of eV Å V^{-1}) and effective polarizabilities (α in units of Å^2 V^{-1}) for methyl species on the Ni(111) surface

Species	$\vec{d}$	α	Species	$\vec{d}$	α
H (fcc)	0.010	0.062	CH_3 (fcc)	−0.191	0.148
C (hcp)	0.066	0.180	CH_2, H (fcc, hcp)	0.059	0.020
CH (fcc)	−0.076	0.193	CH, H (fcc, hcp)	0.063	0.018
CH_2 (fcc)	−0.135	0.157	C, H (fcc, hcp)	0.155	0.036

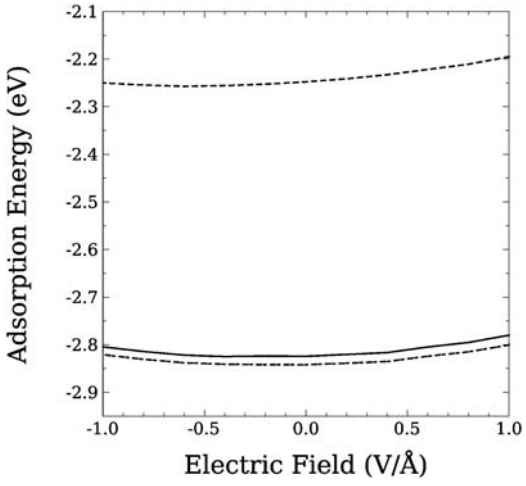

Fig. 2 The effect of an external electric field on the adsorption energy of an H atom on the Ni(111) surface at different adsorbed sites (the top, hcp, fcc sites from top to bottom, respectively).

3.2 Adsorption of hydrocarbon species on Ni(111)

3.2.1 C on a Ni(111) surface. The carbon atom adsorbed onto a Ni(111) surface has three stable adsorption sites, the fcc, hcp and top sites (initial configurations shown in Fig. 1). The most favorable site was the hcp site with an adsorption energy of −6.939 eV and a vertical Ni–C distance of 0.938 Å. This site had a slightly stronger adsorption energy than the fcc site, which had an adsorption energy of −6.883 eV. These small energy differences are similar to those when considering the adsorption of hydrogen. Despite these small energy differences, the designation of the most favorable adsorption site is in agreement with the results of An *et al.*,[12] where the PBE-GGA

functional was used (see Table 1).[26] Finally, the binding energy of the top site was only −4.526 eV, which was significantly weaker than that of the two hollow sites. As was the case for the adsorption of an H atom, the bridge site for the C atom was found to be metastable and it shifted to the nearby fcc site.

Because the external electric fields did not alter the most stable adsorption site for the C atom on the Ni(111) surface, only the electric field effects for a C atom adsorbed at the hcp site will be reported here. Upon addition of the largest positive electric field to this adsorption site (Fig. 3(a)), the adsorption energy increased to −6.784 eV. As the electric field is decreased to −0.4 V Å^{-1}, the adsorption energy reaches its minimum of −6.952 eV, which is 0.013 eV lower than the adsorption energy without an external electric field. The further decrease in the electric field strength produces an increase in the adsorption energy from the minimum found at −0.4 V Å^{-1}. From Fig. 3(a), it is obvious that positive electric fields decrease the adsorption strength much more than negative ones. In addition, we got a positive dipole moment value of 0.066 eV Å V^{-1}. As a result, the adsorption energies were weaker with positive values of the external electric field, which is in line with what was found previously for a single H atom on the Ni(111) surface.

3.2.2 CH on a Ni(111) surface. The next system studied was the adsorption of the CH molecule on the Ni(111) surface. In this case, only the hollow (fcc and hcp) sites proved to be stable (initial configurations shown in Fig. 1). Both the top and bridge sites shifted to the adjacent fcc site. The most favorable adsorption site was found to be the fcc site with an adsorption energy of −6.548 eV, a C–H bond length of 1.100 Å, and a C–Ni distance of 1.132 Å. However, this adsorption site was only 0.02 eV stronger than the hcp site. Wang *et al.*[44] found similar adsorption energies as shown in Table 1. In contrast with the electric field effect on the C atom adsorbed on the Ni(111) surface, the introduction of a large negative electric field of −1.0 V Å^{-1} to CH at the fcc site produces the largest increase in the adsorption energy, up to −6.376 eV. As the electric field is increased, the adsorption strength of CH on this surface increases, reaching an adsorption energy minimum of −6.565 eV at an electric field of 0.4 V Å^{-1}. The values of $|\vec{d}|$ and α are shown in Table 2, which confirms that a negative electric field decreases the stabilities of CH species on a Ni(111) surface.

3.2.3 CH_2 on a Ni(111) surface. Compared to the previous species, Fig. 4 shows six possible configurations studied for the adsorption of CH_2, including two top sites, two bridge sites, one fcc site and one hcp site. All the structures were found to be stable for CH_2 molecules on the Ni(111) surface except the top1 structure (Fig. 4), which shifted to a nearby hcp site. The most favorable site was found to be the fcc site with an adsorption energy of −4.227 eV. As can be seen in Table 1, this fcc site was only 0.05 eV slightly stronger than the hcp site, but much

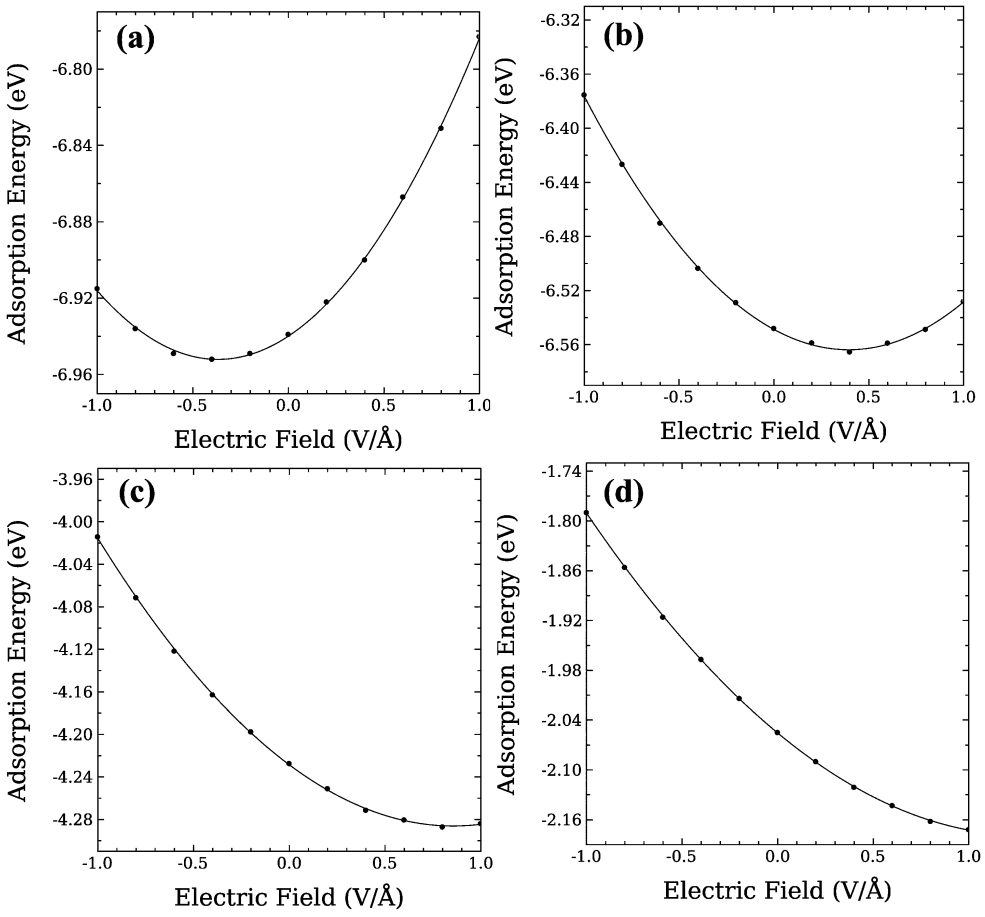

Fig. 3 The effect of an applied external electric field on the adsorption energy of various methyl species adsorbed on the Ni(111) surface. Graphs (a)–(d) show the adsorption energy parabolic trend lines for C, CH, CH_2, and CH_3 species adsorbed on the Ni(111) surface, respectively.

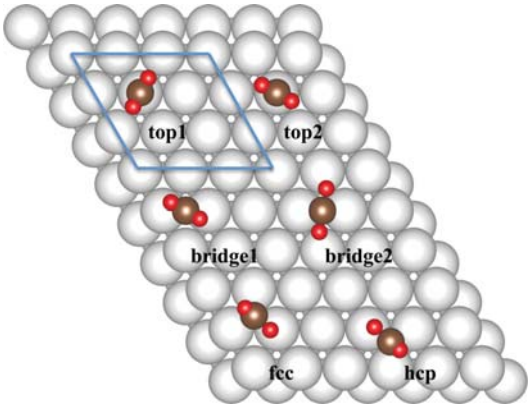

Fig. 4 Top view of the configurations considered for the adsorption of CH_2 molecules on the Ni(111) surface. The top1 site shows the H atoms sit along the line connecting the nearest Ni atoms while the H atoms sit along the line connecting the hollow sites of Ni atoms for top2. The bridge1 site has the H atoms along the line connecting the two nearest neighbor surface atoms while the bridge 2 site has the H atoms sitting along the line that connect the two diagonal Ni surface atoms.

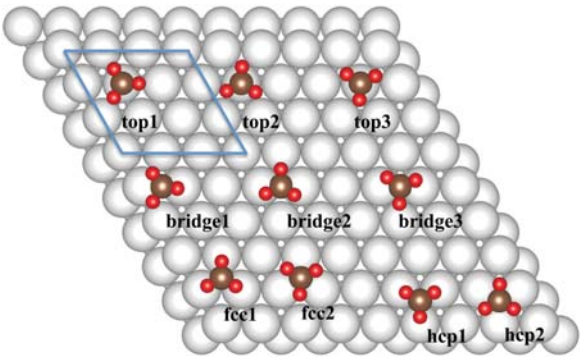

Fig. 5 Top view of the adsorption configurations of CH_3 on the Ni(111) surface. The H atom of the top1 position lies along the lines connecting three nearest neighbor Ni surface atoms. The H atoms of the top2 and top3 structures sit at the hcp and fcc sites adjacent to the carbon bonded top site, respectively. The bridge1 site has a single H atom lying on the top of a Ni surface atom. The bridge2 and bridge3 configurations differ from each other and the bridge1 configuration in that a single H lies on an fcc site and hcp site, respectively. The two possible configurations for each the fcc and hcp sites show all of the H atoms either in top or hollow sites.

stronger than CH_2 on the bridge1, bridge2 and top2 sites. It is worth noting that the adsorbed geometry of a CH_2 molecule is not symmetric at the fcc and hcp sites, but symmetric at the top and bridge sites. As for the CH_2 molecule at the hollow sites, the shorter C–H bond length is 1.101 Å and the longer one is 1.164 Å, which plays an important role in the study of the transition state for the decomposition of CH_2. These results show excellent agreement with results of Watwe *et al.*,[19] where CH_2 on a $p(2 \times 2)$ supercell prefers a threefold hollow site to the bridge site by −0.207 eV.

In addition to the above work, the effects of an external electric field in this system were examined and are given in Fig. 3(c). Comparing the different external electric field effects on the adsorption energy of the CH_2 molecule on the Ni(111) surface, it is clear that when an electric field of 0.8 V $Å^{-1}$ was applied, the adsorption energy between the CH_2 molecule and Ni slab was minimized. The presence of stronger electric fields, −1.0 or 1.0 V $Å^{-1}$, increases its adsorption energy from its minimal value to −4.014 and −4.284 eV, respectively. Approximating these adsorption energies by a quadratic function gives a large negative dipole moment, −0.135 eV Å V^{-1}.

3.2.4 CH_3 on a Ni(111) surface. The adsorption of CH_3 on the Ni(111) surfaces shows more variation than the H, C, CH, and CH_2 species with respect to their binding sites. For the adsorption on the top and bridge sites, three orientations were considered where the C–H bonds are aligned with adjacent Ni atoms, the fcc or hcp sites. For the carbon adsorbed onto the fcc and hcp sites, two orientations were calculated where the C–H bonds are aligned with adjacent top and hollow sites. These various orientations of CH_3 are shown Fig. 5. After the optimization of each of these configurations, only the top1, top2, top3, bridge1, fcc1, and hcp1 sites were stable. It was found that the most stable adsorption position was the fcc1 site, with an adsorption energy of −2.055 eV and bond lengths of 1.120, 1.118, 1.119 Å for the three C–H bonds, respectively. Like the case of the adsorption of CH_2, this favored adsorption site had only a slight adsorption preference over the hcp1 site. The bridge1, top1, top2 and top3 sites were found to be less stable than the hollow sites and these three orientations of top sites have the same adsorption energy. Nave *et al.*[47] also investigated the adsorption energy of methyl species considering the same orientations, and found similar results for the adsorption energy of CH_3 as can be seen by examining Table 1.

When electric fields, ranging from 1.0 V $Å^{-1}$ to −1.0 V $Å^{-1}$, were applied in this system with the CH_3 molecule adsorbed onto the most favorable fcc site (shown in Fig. 3(d)), the adsorption energy of this system decreased monotonically from −1.790 at −1.0 V $Å^{-1}$ to −2.172 eV at 1.0 V $Å^{-1}$. When fitting this to a parabolic equation, we obtain the values of $|\vec{d}|$ and α as given in Table 2. This electric field effect is similar to the effect on CH_2 species, where positive electric fields make the system more stable and negative ones weaken the adsorption energy of CH_3.

Overall, the presence of a large external electric field on the adsorption of methyl species at the most favorable sites on a Ni(111) surface causes the adsorption energy to fluctuate around 0.2 eV. However, the geometries of the hydrocarbon species, including C–H bond distances, H–C–H bond angles, and favorable sites for the adsorbed species were not significantly altered by the presence of an electric field. Results of the adsorption energies of methyl species without an external electric field are summarized in Table 1, and results of the dipole moments $\vec{d}$ and effective polarizabilities α are shown in Table 2.

3.3 Co-adsorption of CH_x species and an H atom on a Ni(111) surface

In order to get the minimum energy pathways (MEP) and energy barriers of the methyl three-stepped dissociative reactions on a Ni(111) surface, we need to find the initial image and final image configurations that have the lowest co-adsorption reaction energy. Based on the adsorption energy results of the isolated hydrocarbon species adsorbed on a Ni(111) surface, we have already ensured that the initial images for each of the reaction

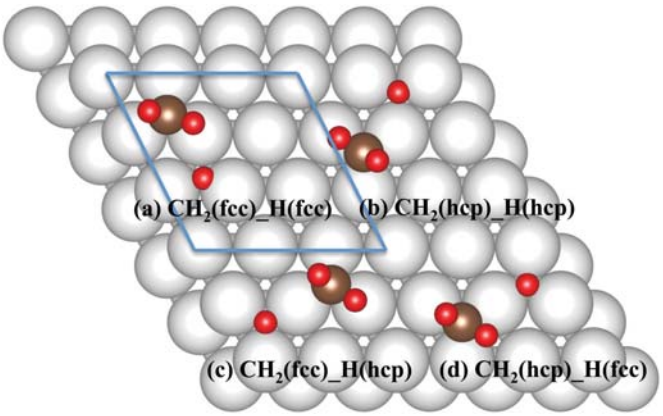

Fig. 6 The configurations considered for the different co-adsorption sites of CH_2 and an H atom on the Ni(111) surface. CH_2 molecules were then systematically replaced by CH and C species in order to calculate the co-adsorption reaction energies of CH and H species or C and H species.

pathways are known. The second step was to determine the lowest co-adsorption configuration of the methyl species and an H atom on the Ni(111) surface so as to find the final images for each reaction pathway.

3.3.1 CH_2 and H co-adsorbed on a Ni(111) surface. Since the most stable sites for CH_2 and H are both at the fcc sites with the binding energy of the hcp sites of these atoms being only slightly weaker than the fcc sites, four possible co-adsorbed configurations with mixtures of both adsorption sites were considered (these co-adsorbed configurations and calculation results are shown in Fig. 6 and Table 3). From the results, it is clear that the lowest co-adsorption reaction energy structure for the CH_2 and H species on the Ni(111) surface is the CH_2 at the fcc site and an H atom at the hcp site with a co-adsorption reaction energy of 0.064 eV. The corresponding bond distance between the co-adsorbed H atom and the C atom is 2.979 Å, which is therefore the final image for the decomposition of CH_3. The other co-adsorbed cases have a slight increase in the co-adsorption reaction energies, which are given in Table 3. All the separate reaction energies were found to have positive values, indicating this reaction is endothermic. Moreover, when we apply an electric field on the configuration having a CH_2 molecule at an fcc site co-adsorbed with an H atom at an hcp site, we find that the co-adsorption reaction energy monotonically increases from 0.015 eV to 0.133 eV when the external field is varied from -1.0 V Å^{-1} to 1.0 V Å^{-1} (see Fig. 7(a)). As for the dipole moment, its positive value given in Table 2 verifies that an applied external positive electric field results in weaker co-adsorption energies of CH_2 and H. Furthermore, the geometries of the co-adsorbed CH_2 and H species, including the distance between the C and the isolated H atom, the binding distance between Ni and C, and Ni and the isolated H atom, were not altered by the applied electric fields.

3.3.2 CH and H co-adsorbed on a Ni(111) surface. The co-adsorption sites for the CH and H species were studied in the same manner as those for CH_2 and H (Fig. 6), since CH_2 and CH have the similar site preferences. The most favorable co-adsorbed site was found to be CH at the fcc site and H at the nearby hcp site, which had the lowest co-adsorption reaction energy of -0.360 eV. The co-adsorption energies of CH and H both at the hcp sites, CH and H both at the fcc sites, and CH at the hcp site and H at the nearby fcc site were slightly higher than the most stable one, with co-adsorption energies shown in Table 3. From Table 3, it is clear that the separate reaction energy of $CH_2^* \rightarrow CH^* + H^*$ is exothermic regardless of the adsorbed sites. Fig. 7(b) shows the electric field effect on the co-adsorption reaction for the most stable structure. The co-adsorbed reaction energy goes up monotonically with positive electric fields to -0.288 eV at a field value of 1.0 V Å^{-1} and decreases to a minimum of -0.414 eV at an electric field value of -1.0 V Å^{-1}. As was the case for the co-adsorption of CH_2 and H species on Ni(111), an external positive electric field weakens the co-adsorption reaction energy of the CH and H species.

3.3.3 C and H co-adsorbed on a Ni(111) surface. These simulations were conducted as described above (Fig. 6) and we found that the C atom at the fcc site and the H atom at the adjacent hcp site had the lowest co-adsorption reaction energy of 0.548 eV. This final configuration will be used to determine the MEP for this decomposition. Since the co-adsorption reaction energy of the CH molecule at the hcp site is only 0.02 eV weaker than that at the fcc site, we will also investigate another reaction pathway starting from the CH species at the hcp site, giving a C at the same hcp site and an H atom at the adjacent hcp site so that the reaction proceeds as:

$$CH^*(hcp) \rightarrow C^*(hcp) + H^*(hcp) \quad (10)$$

The electric field will have a significantly larger effect on the C and H co-adsorbed on the Ni(111) surface than those found for the previous two dissociative reactions. When a positive electric field of 1.0 V Å^{-1} is applied, the co-adsorption reaction energy of:

$$CH^*(fcc) \rightarrow C^*(fcc) + H^*(hcp) \quad (11)$$

Table 3 Summary of the co-adsorption reaction energy data and separate reaction energy of methyl species and H atom

Species	E_c (eV)	E_s (eV)	Species	E_c (eV)	E_s (eV)
CH_2, H (fcc, fcc)	0.188	0.047, 0.056[a], 0.04[b]	CH, H (fcc, hcp)	−0.360, −0.282[a]	−0.340
CH_2, H (hcp, hcp)	0.165	0.116	CH, H (hcp, fcc)	−0.359, −0.28[c]	−0.344, −0.442[a]
CH_2, H (fcc, hcp)	0.064, 0.356[a], 0.36[c]	0.064	C, H (fcc, fcc)	0.612	0.524
CH_2, H (hcp, fcc)	0.095	0.098	C, H (hcp, hcp)	0.581, 0.837[a], 0.84[c]	0.486
CH, H (fcc, fcc)	−0.308	−0.358, −0.37[b]	C, H (fcc, hcp)	0.548	0.542
CH, H (hcp, hcp)	−0.278	−0.326	C, H (hcp, fcc)	0.581	0.468, 0.503[a], 0.45[b]

[a] From ref. 15. [b] From ref. 36. [c] From ref. 48.

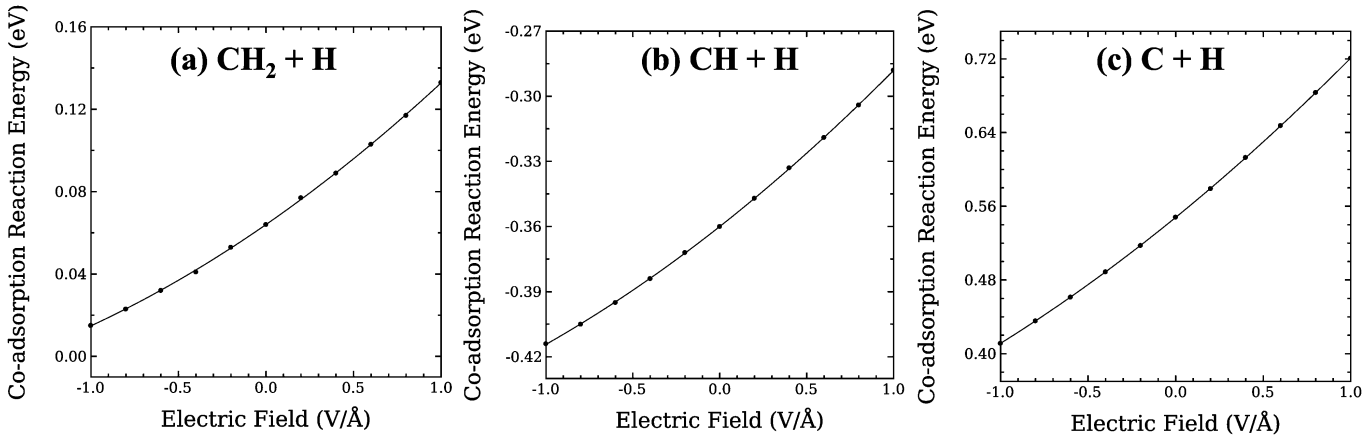

Fig. 7 The effects of an external electric field on the co-adsorption reaction energies of CH_x and H species on the Ni(111) surface. (a) represents the co-adsorption reaction energy of CH_2 at the fcc site and H at the nearby hcp site. The co-adsorption reaction energy of a CH molecule at the fcc site and an H atom at the neighboring hcp site is given in (b). Finally, (c) shows the co-adsorption reaction energy of a C atom at the fcc site and an H atom at the adjacent hcp site.

increases to 0.721 eV. On the other hand, the co-adsorption reaction energy decreases to 0.411 eV in the presence of a negative electric field of -1.0 V Å^{-1}. The overall effect of the various electric fields on the co-adsorbed reaction energy is around 0.310 eV, which is larger than the effects found on the CH_3 and CH_2 decomposition steps. For the reaction given in eqn (10), the co-adsorption reaction energy varied from 0.736 eV to 0.436 eV when applying electric fields of 1.0 V Å^{-1} and -1.0 V Å^{-1}, which again is higher than the co-adsorption reaction energies of CH_2 and CH co-adsorbed with H species.

3.4 Transition state and energy barriers

3.4.1 Reaction pathway: CH_3*(fcc) → CH_2*(fcc) + H*(fcc) → CH_2*(fcc) + H*(hcp). The dissociative reaction of CH_3 at the fcc site into a CH_2 molecule at the fcc site and an H atom at the neighboring hcp site was found to go through an intermediate minimum. This intermediate configuration had CH_2 and H adsorbed into two adjacent fcc sites (the MEP of the dehydrogenation of CH_3 in the presence and absence of the electric fields are shown in Fig. 8). To address this problem, the reaction pathway was separated into two segments. The energy barrier for the first pathway of CH_3*(fcc) → CH_2*(fcc) + H*(fcc) was found to be 0.692 eV as can be seen in Table 4. This barrier was nearly 0.6 eV higher than the one found for the second pathway of CH_2*(fcc) + H*(fcc) → CH_2*(fcc) + H*(hcp). The first energy barrier leads to a product state having a co-adsorption reaction energy of 0.106 eV above the reactant with the CH_2 product bonded at the fcc site and the H at the nearby fcc site. In the

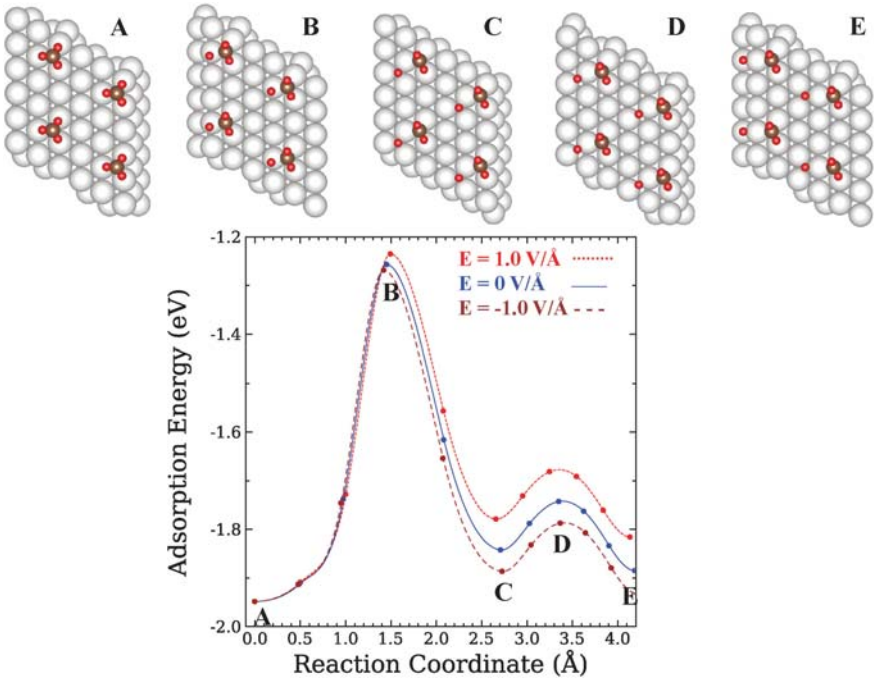

Fig. 8 The MEP of the CH_3*(fcc) → CH_2*(fcc) + H*(fcc) → CH_2*(fcc) + H*(hcp) reaction both with and without an external electric field.

Table 4 Summary of the electric field effects on the energy barriers of dehydrogenation reactions of CH_x species on the Ni(111) surface

Reaction paths	Transition state	Energy barriers (eV)
CH_3*(fcc) → CH_2*(fcc) + H*(fcc)	CH_2 (fcc), H (top)	0.713/0.692 (0.798[a], 0.78[b])/0.680
CH_2*(fcc) + H*(fcc) → CH_2*(fcc) + H*(hcp)	CH_2 (fcc), H (bridge)	0.098/0.100/0.099
CH_2*(fcc) → CH*(fcc) + H*(hcp)	CH (fcc), H (top)	0.349/0.323 (0.360[a], 0.37[b])/0.304
CH*(fcc) → C*(fcc) + H*(hcp)	C (fcc), H (top)	1.494/1.373 (1.36[b])/1.271
CH*(hcp) → C*(hcp) + H*(hcp)	C (hcp), H (bridge)	1.427/1.287 (1.422[a])/1.185

Energy barriers in the presence of a positive electric field of 1.0 V Å^{-1}, in the absence of a field and with a negative electric field of −1.0 V Å^{-1}, respectively. Reference energy barrier values in the absence of a field are given in parentheses. [a] From ref. 15. [b] From ref. 35.

second pathway, the H atom shifts to the nearby hcp position, which lowers the energy of the previous product so that this reaction is exothermic with a co-adsorption reaction energy of −0.043 eV.

During the first pathway for the dissociative reaction of CH_3, the transition state shows that the H atom sits near the top site, forming a bond with the Ni atom below. The bond distance between H and Ni was found to be 1.494 Å, which is similar to the bond distance of 1.470 Å for an isolated H atom binding at the top site. The bond length of the carbon atom and this active hydrogen increased to 1.754 Å at the transition state, which is well over the C–H bond length (1.119 Å) in the CH_3 molecule. This suggests that the C–H bond has already been broken at the transition state. As the C–H bond breaks, the H atom forms a bond with a Ni atom at the corner of the fcc site and then moves to the nearby fcc site. During the second separate segment, the active H atom goes from the fcc site to the final hcp site though a bridge site. The second transition state occurs when the H atom lies at the bridge site and the CH_2 molecule stays at the fcc site with a smaller energy barrier of 0.100 eV.

We applied large external positive electric fields of 1.0 V Å^{-1} and −1.0 V Å^{-1} to understand its influence on the underlying reaction. When we apply a positive electric field, the first energy barrier goes up to 0.713 eV, 0.021 eV higher than the one without an external electric field. A negative electric field causes the first energy barrier to go down by 0.012 eV to 0.680 eV. Finally, the geometric configuration for the TS is not affected at the presence of an external electric field. Therefore, the external electric field effect on the energy barriers involved in the reaction CH_3*(fcc) → CH_2*(fcc) + H*(fcc) → CH_2*(fcc) + H*(hcp) is not significant.

3.4.2 Reaction pathway: CH_2*(fcc) → CH*(fcc) + H*(hcp). The next step in the dehydrogenation of CH_3 is the further decomposition of CH_2 as CH_2* → CH* + H*. The reaction proceeds from the initial image of CH_2 at the fcc site through the breaking of the shorter C–H bond, where a CH molecule is found at the fcc site and a H atom at a nearby hcp site (Fig. 9). Compared to the reactant, the final product has a significantly lower energy, so that the reaction is exothermic with the co-adsorption reaction energy of −0.360 eV.

At the transition state, the H is at a top site with a Ni–H bond length of 1.481 Å and the CH molecule is at a fcc site with an energy barrier as given in Table 4. Moreover, the bond length between C and the leaving H atom is 1.699 Å, suggesting that the C–H bond has already been broken. As before, we applied different, large electric fields and studied the effects on this

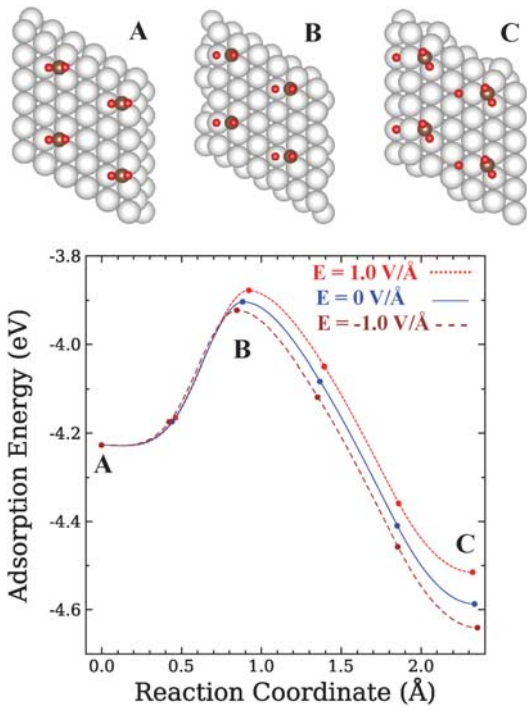

Fig. 9 The CH_2 dissociation pathway, starting from an fcc site, and ending with the CH molecule at the same fcc site and the dissociated H at the nearby hcp site.

exothermic reaction. The energy barrier increased by 0.026 eV in the presence of a positive electric field of 1.0 V Å^{-1}. On the other hand, the energy barrier decreased by 0.019 eV in the presence of a negative electric field of −1.0 V Å^{-1}. Once again, the external electric field minimally affects the energy barriers involved in the decomposition of the CH_2 species on the Ni(111) surface.

3.4.3 Reaction pathway: CH*(fcc) → C*(fcc) + H*(hcp). The final step for the decomposition of the CH_3 species on a Ni(111) surface is CH* → C* + H*. We found that the lowest energy pathway for this decomposition has an energy barrier of 1.373 eV (Fig. 10(a)). The conversion of the CH species at the fcc site on the Ni(111) surface to C and H atoms has a considerably large energy barrier, as compared to the other two elementary dissociative reactions. When the product is formed, the C is bonded at the same fcc site and the H binds at an adjacent hcp site (see Fig. 10(a)). This system has the co-adsorption reaction energy of 0.548 eV higher than the CH reactant, indicating that this step is an endothermic reaction and is the rate-limiting step in the dehydrogenation of methyl groups.

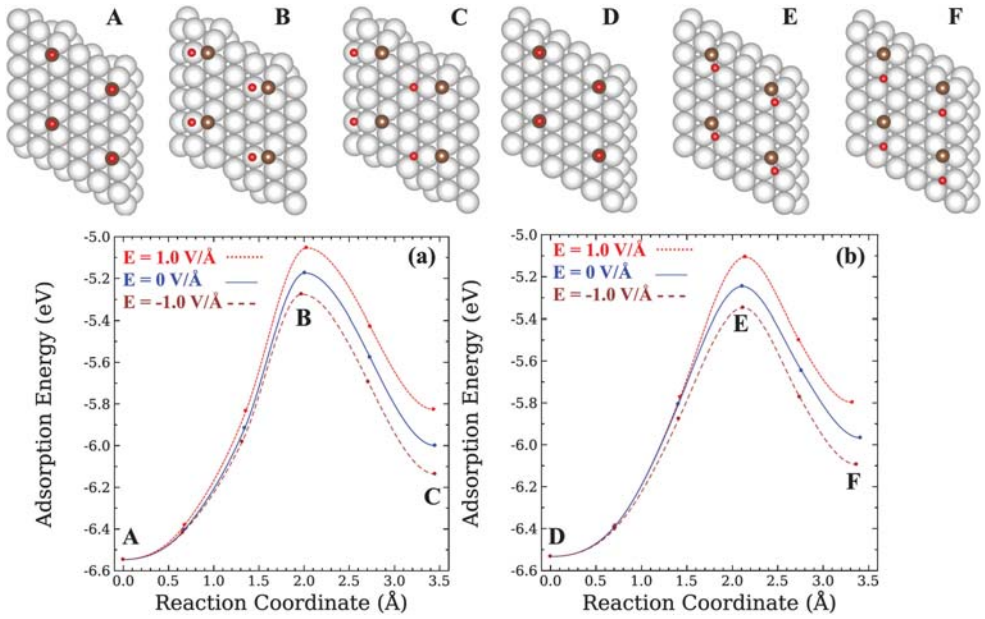

Fig. 10 The dissociation pathway for a CH molecule, starting from different initial adsorbed sites. Part (a) starting from the fcc site and part (b) starting from the hcp site.

The transition state for this endothermic reaction has the C at the fcc site and the H atom at the nearby top position. The bond length of C and the corresponding fcc Ni atom was found to be 5.127 Å, which is similar to the bond distance of 5.102 Å when the isolated C atom is adsorbed at the fcc site on the Ni(111) surface. The H atom is on the top of a Ni surface atom with a bond distance of 1.492 Å, which is identical to an isolated H atom bound at a top site. Moreover, the C–H distance has increased to 1.781 Å. When we introduced a positive electric field of 1.0 V $Å^{-1}$, the energy barrier increases by 0.121 eV, which is six times stronger than that found in the previous reactions. In other words, a positive electric field makes the conversion of CH species to C atoms much more difficult than the previous reactions, suggesting that pure carbon is much harder to form on the Ni(111) surface. This effect indirectly suppresses the carbon–carbon bonds formation on the Ni active surface to some extent. We also studied the effect of applying a negative electric field in this system and found that the energy barrier decreased by 0.102 eV, which is again a significantly higher effect as compared to the previous reactions. From these results, the addition of external electric fields plays a significant role in the decomposition of the CH molecule on the Ni(111) surface.

3.4.4 Reaction pathway: CH*(hcp) → C*(hcp) + H*(hcp). Since the adsorption energy of CH at the hcp site is only 0.014 eV weaker than that found on the fcc site, another reaction pathway of dissociation of CH was considered (Fig. 10(b)). This reaction starts from a CH molecule at the hcp site and goes to the final image, where C stays at the hcp site and the H atom shifts to an adjacent hcp site. The transition state occurs when the H is at the bridge site and C at the nearby hcp site with the energy barrier of 1.287 eV. In addition, we also investigated the electric field effect on this particular reaction. The energy barrier was 1.427 eV when an electric field 1.0 V $Å^{-1}$ is applied and decreased to 1.185 eV in the presence of a negative electric field of −1.0 V $Å^{-1}$.

3.4.5 Summary of dehydrogenation of methyl species. Fig. 11 shows the reaction barriers and dissociation reaction energies for the CH_3 species' dehydrogenation on a Ni(111) surface to form in sequence CH_2* + H*, CH* + 2H*, and C* + 3H*.

Here we assume that the H atoms diffuse away from the CH_x species on the surface. In particular, CH_3 at an fcc site goes through the TS1 transition state which leads to the formation of CH_2 and H, which will be infinitely separated from one another at their most favorable adsorption sites. Similarly, CH_2 and CH species pass through TS2 and TS3 and generate isolated CH and H followed by isolated C and H adsorbates. These dissociation reactions can be summarized as in eqn (12):

$$CH_3 + (4 - x)^* \rightarrow CH_x^* + (3 - x)H^* \quad (12)$$

The dissociation reaction energy was calculated by using eqn (13):

$$E_{diss} = [E_{(CH_x/slab)} + (3 - x)E_{(H/slab)}] - [(4 - x)E_{(slab)} + E_{(CH_3)}] \quad (13)$$

when x equals 3, the dissociation reaction energy is the same as the adsorption energy of the CH_3 molecule. We remark that a similar definition for the dissociation reaction energy has been used in the literature[44] when considering the adsorption of methane on several Ni single crystal surfaces.

Using eqn (13) and the barriers given in Table 4, we have plotted the dissociation reaction energies and energy barriers for all the reaction intermediates in Fig. 11 in the presence and in the absence of an external electric field. The presence of a field clearly affects the relative stability of reactants and the products. In particular, the adsorption energy of a CH_3 molecule in the presence of a positive electric field is significantly enhanced. This shows that while the electric field effect on the

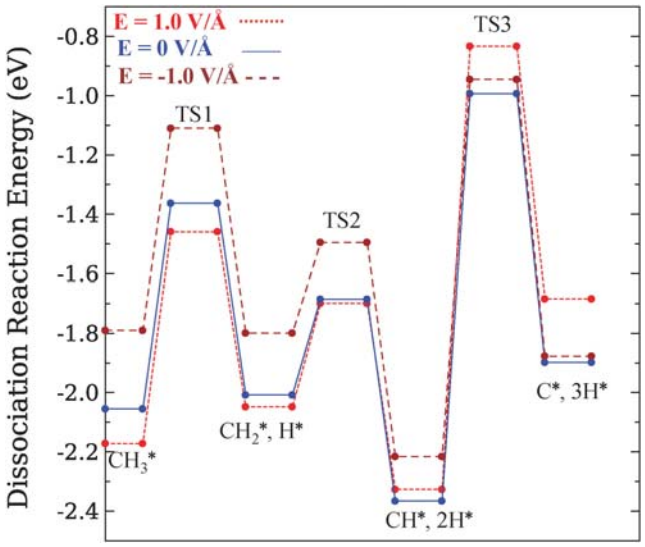

Fig. 11 Energy pathway for CH_3 decomposition to C and H on the Ni(111) surface in the presence and absence of an external electric field. TS1, TS2 and TS3 stand for the transition state of the decomposition of CH_3, CH_2 and CH species, respectively.

individual reaction barriers is small, the overall decomposition reaction of CH_3 to surface CH_2 and H is significantly enhanced in the presence of a positive external electric field.

From Fig. 11 we can also see that the TS3 transition state has the highest energy barrier, meaning that the dehydrogenation of the CH species is the rate-limiting step for this reaction on the Ni(111) surface. When we applied a positive external electric field of 1.0 V $Å^{-1}$, we find that the CH dehydrogenation energy barrier increased by 0.121 eV, which is six times higher than the electric field effect on the barriers for the other reactions. Moreover, a positive electric field weakens the dissociation reaction energy for the formation of C* and 3H* on the surface. Therefore, one can conclude that the positive electric field suppresses the formation of pure carbon on the Ni(111) surface while promoting the dissociation of the CH_3 species.

4. Conclusions

An investigation of the CH_x species adsorption and co-adsorption of methyl species on a clean Ni(111) surface in the presence and the absence of an external electric field was performed. The presence of an external electric field within these systems does not affect the geometries of the adsorbed species and the favorable adsorption sites. For the isolated species, the external electric field effects for H and C groups are similar, where the adsorption energy increases in the presence of a positive electric field and decreases to a minimum when the electric field is -0.4 V $Å^{-1}$. The CH, CH_2, and CH_3 species respond in a similar manner in the presence of the external electric fields, where the adsorption energy increases by applying a negative electric field and has a minimum when the electric field is 0.4 V $Å^{-1}$. For the electric field effect on the co-adsorption species, positive electric fields were found to stabilize the co-adsorbed species and the negative electric fields were found to weaken the adsorption strength of the co-adsorbed species.

In addition to this work, we examined the minimum energy pathways, the transition states and energy barriers in the decomposition of CH_3 on the Ni(111) surface. The MEP for the whole dehydrogenation reaction of CH_3 to C is as follows. The CH_3 molecule initially binds to the fcc site and a single H atom detaches from the CH_3 molecule. The H atom moves to a nearby hcp site and CH_2 stays at the original fcc site. Next, the CH_2 further loses an H atom by breaking the shorter C–H bond and separating the active H to the neighboring hcp site, leaving the CH molecule at the fcc site. Finally, the bond of the CH molecule is broken, leaving the C atom at the fcc site and shifting the active hydrogen atom to an adjacent hcp site. We also found that the energy barriers decrease when a negative external electric field is applied. However, when we apply a positive electric field, the energy barriers of these dissociative reactions of CH_x all increase. Particularly, for the dehydrogenation of CH species, the energy barrier increases more significantly than the other reactions, suggesting that a positive electric field will impede the CH* → C* + H* reaction. As a result, this will directly decrease the pure C atoms produced by the decomposition of the CH_3 species and to some degree suppress the formation of coke on the Ni(111) surface.

Acknowledgements

This work was supported by institutional funds provided to JSM from the Voiland School of Chemical Engineering and Bioengineering and by the American Chemical Society Petroleum Research Fund under grant number 52769-DNI5.

References

1 E. W. Park, H. Moon, M. S. Park and S. H. Hyun, *Int. J. Hydrogen Energy*, 2009, **34**, 5537–5545.
2 B. C. H. Steele, *Nature*, 1999, **400**, 619–621.
3 M. d. Ridder, R. G. v. Welzenis, H. H. Brongersma, S. Wulff, W. F. Chu and W. Weppner, *Nucl. Instrum. Methods Phys. Res., Sect. B*, 2002, **190**, 732–735.
4 M. Jiang, W. Michael Griffin, C. Hendrickson, P. Jaramillo, J. VanBriesen and A. Venkatesh, *Environ. Res. Lett.*, 2011, **6**, 034014–034024.
5 T. A. Adams Ii and P. I. Barton, *Fuel Process. Technol.*, 2011, **92**, 2105–2115.
6 H. Mulchandani and A. R. Brandt, *Energy Fuels*, 2011, **25**, 1633–1641.
7 M. Vandenbossche and S. McIntosh, *J. Catal.*, 2008, **255**, 313–323.
8 T. V. Choudhary and D. W. Goodman, *J. Mol. Catal. A: Chem.*, 2000, **163**, 9–18.
9 R. Oza and S. Patel, *Res. J. Recent Sci.*, 2012, **1**, 434–443.
10 Z. G. Hao, Q. S. Zhao, Z. Jiang, B. L. Hou and H. Z. Li, *Fuel Process. Technol.*, 2009, **90**, 113–121.
11 M. N. Barroso, A. E. Galetti and M. C. Abello, *Appl. Catal., A*, 2011, **394**, 124–131.
12 W. An, X. C. Zeng and C. H. Turner, *J. Chem. Phys.*, 2009, **131**, 174702.

13 H. Liu, R. Zhang, R. Yan, J. Li, B. Wang and K. Xie, *Appl. Surf. Sci.*, 2012, **258**, 8177–8184.
14 T. P. Beebe, D. W. Goodman, B. D. Kay and J. T. Yates, *J. Chem. Phys.*, 1987, **87**, 2305–2315.
15 J. E. Mueller, A. C. T. v. Duin and W. A. Goddard, *J. Phys. Chem. C*, 2009, **113**, 20290–20306.
16 S. Nave and B. Jackson, *J. Chem. Phys.*, 2007, **127**, 224702.
17 P. Kratzer, B. Hammer and J. K. Nørskov, *J. Chem. Phys.*, 1996, **105**, 5595–5604.
18 H. S. Bengaard, J. K. Nørskov, J. Sehested, B. S. Clausen, L. P. Nielsen, A. M. Molenbroek and J. R. Rostrup-Nielsen, *J. Catal.*, 2002, **209**, 365–384.
19 R. M. Watwe, H. S. Bengaard, J. R. Rostrup-Nielsen, J. A. Dumesic and J. K. Nørskov, *J. Catal.*, 2000, **189**, 16–30.
20 Q. Y. Yang, K. J. Maynard, A. D. Johnson and S. T. Ceyer, *J. Chem. Phys.*, 1995, **102**, 7734–7750.
21 E. M. Stuve, *Chem. Phys. Lett.*, 2012, **519–520**, 1–17.
22 R. M. Ormerod, *Chem. Soc. Rev.*, 2003, **32**, 17–28.
23 G. S. Karlberg, J. Rossmeisl and J. K. Nørskov, *Phys. Chem. Chem. Phys.*, 2007, **9**, 5158–5161.
24 E. Nikolla, J. Schwank and S. Linic, *J. Electrochem. Soc.*, 2009, **156**, B1312–B1316.
25 J. White and D. Bird, *Phys. Rev. B: Condens. Matter Mater. Phys.*, 1994, **50**, 4954–4957.
26 J. P. Perdew, K. Burke and M. Ernzerhof, *Phys. Rev. Lett.*, 1996, **77**, 3865–3869.
27 J. P. Perdew and Y. Wang, *Phys. Rev. B: Condens. Matter Mater. Phys.*, 1992, **45**, 13244–13249.
28 M. C. Payne, T. A. Arias and J. D. Joannopoulos, *Rev. Mod. Phys.*, 1992, **64**, 1045–1097.
29 G. H. Golub and D. P. O'Leary, *J. Soc. Ind. Appl. Math.*, 1989, **31**, 50–102.
30 S. G. Wang, D. B. Cao, Y. W. Li, J. G. Wang and H. J. Jiao, *J. Phys. Chem. B*, 2005, **109**, 18956–18963.
31 F. A. Pedersen, J. Greeley and J. K. Nørskov, *Catal. Lett.*, 2005, **105**, 9–13.
32 A. Michaelides and P. Hu, *Surf. Sci.*, 1999, **437**, 362–376.
33 Y. C. Huang, J. Y. Du, C. Y. Ling, T. Zhou and S. F. Wang, *Catal. Sci. Technol.*, 2013, **3**, 1343–1355.
34 A. A. Phatak, W. N. Delgass, F. H. Ribeiro and W. F. Schneider, *J. Phys. Chem. C*, 2009, **113**, 7269–7276.
35 H. Y. Liu, R. X. Yan, R. G. Zhang, B. J. Wang and K. C. Xie, *J. Nat. Gas Chem.*, 2011, **20**, 611–617.
36 Y. Xu, C. Fan, Y. A. Zhu, P. Li, X. G. Zhou, D. Chen and W. K. Yuan, *Catal. Today*, 2012, **186**, 54–62.
37 H. J. Monkhorst and J. D. Pack, *Phys. Rev. B: Solid State*, 1976, **13**, 5188–5192.
38 S. G. Louie, S. Froyen and M. L. Cohen, *Phys. Rev. B: Condens. Matter Mater. Phys.*, 1982, **26**, 1738–1742.
39 H. Jónsson, G. Mills and K. W. Jacobsen, *Nudged elastic band method for finding minimum energy paths of transitions*, 1998, vol. 16, p. 385.
40 G. Henkelman and H. Jónsson, *J. Chem. Phys.*, 1999, **111**, 7010–7023.
41 G. Henkelman, B. P. Uberuaga and H. Jónsson, *J. Chem. Phys.*, 2000, **113**, 9901–9904.
42 S. A. Trygubenko and D. J. Wales, *J. Chem. Phys.*, 2004, **120**, 2082–2094.
43 G. Henkelman, A. Arnaldsson and H. Jónsson, *J. Chem. Phys.*, 2006, **124**, 044706.
44 S. G. Wang, D. B. Cao, Y. W. Li, J. G. Wang and H. J. Jiao, *Surf. Sci.*, 2006, **600**, 3226–3234.
45 K. Christmann, R. J. Behm, G. Ertl, M. A. Van Hove and W. H. Weinberg, *J. Chem. Phys.*, 1979, **70**, 4168–4184.
46 J.-S. McEwen, P. Gaspard, T. Visart de Bocarmé and N. Kruse, *J. Phys. Chem. C*, 2009, **113**, 17045–17058.
47 S. Nave and B. Jackson, *J. Chem. Phys.*, 2009, **130**, 054701.
48 M. Pozzo, G. Carlini, R. Rosei and D. Alfe, *J. Chem. Phys.*, 2007, **126**, 164706.

